II International Conference on Simulation for Additive Manufacturing - Sim-AM 2019
F. Auricchio, E. Rank, P. Steinmann, S. Kollmannsberger and S. Morganti (Eds)

A MESOSCOPIC APPROACH FOR MODELLING LASER BEAM MELTING (LBM)

YAASIN A. MAYI[1, 3], MORGAN DAL[1], PATRICE PEYRE[1], MICHEL BELLET[2], CHARLOTTE METTON[3], CLARA MORICONI[3], RÉMY FABBRO[1]

[1] Laboratoire PIMM, Arts et Métiers, CNRS, Cnam, HESAM Université
151 Bd de l'hôpital 75013 Paris, France
e-mail: yaasin.mayi@protonmail.com, web page: https://pimm.artsetmetiers.fr

[2] CEMEF, UR 7635 PSL Research University MINES ParisTech
06904 Sophia Antipolis, France
web page: http://www.cemef.mines-paristech.fr

[3] Safran Additive Manufacturing, a technology platform of Safran Tech
Rue des Jeunes Bois, Châteaufort, 78114 Magny-Les-Hameaux, France
web page: https://www.safran-group.com

Key words: Laser Beam Melting (LBM), Powder Bed Fusion (PBF), Selective Laser Melting (SLM), additive manufacturing, laser-matter interaction, Arbitrary Lagrangian Eulerian (ALE).

Summary: *Laser Beam Melting (LBM) is currently garnering industrial attention and many numerical researches have been carried out in order to understand the physics behind the process. However, due to the gap between the grain scale (micrometres) and the bead scale (millimetres), current state-of-the-art multi-physical models are computationally expensive as each powder grain is individually represented. Hence, simulating more than a single LBM track in a reasonable computational time is a challenging task. To overcome this limitation, a new mesoscopic approach is proposed, which intends to bridge the fine thermo-hydrodynamic representation and the macroscopic thermal models. The powder bed is represented by a homogeneous medium with both equivalent thermal and fluid properties. A bulk heat source is considered when the laser heats the powder bed whereas a surface heat flux is imposed on the melted powder bed surface. Apparent viscosity and surface tension are attributed to the homogenized medium so that modelling powder densification, melting and spheroidization of the melt pool is made possible by solving compressible Navier-Stokes equations. In addition, thermocapillary effects as well as vaporisation-induced recoil pressure are implemented, so that realistic thermo-hydrodynamic phenomena are successfully taken into account.*

1 INTRODUCTION

Laser Beam Melting (LBM) is an additive manufacturing process where successive layers of metallic powder are selectively melted by a laser beam, following a computer-programmed strategy. This technology is garnering an important industrial attention, especially in the aerospace sector, as it gives design flexibility that brings the opportunity to think differently the shape and the functionalities of manufactured components. The interaction between the laser beam and the powder bed gives rise to complex physical phenomena (energy absorption by the powder, melting, melt pool convection, metal vaporisation, rapid solidification and so on)

which must be understood to control the process at the industrial scale. In this regard, multi-physical simulation of laser-material interaction becomes an essential research tool to complete experimental diagnostics, to help understanding the origin of some defects such as porosities or cracks and to predict solidification conditions.

However, due to the gap between the grain scale (micrometres) and the bead scale (millimetres), numerical simulation of LBM leads to the use of important computational resources. Generally, to bypass this limitation, two simulation strategies are encountered [1,2]. Firstly, at the micro/mesoscale, the models are focused on the laser-matter interaction and on the thermo-hydrodynamic phenomena involved at the vicinity of the melt pool. Current state-of-the-art multi-physical models are still computationally expensive as each powder grain is individually represented [3,4]. Hence, simulating more than a single LBM track in a reasonable computational time is a challenging task. Secondly, at the macroscale, the models are interested in the thermomechanical behaviour of the component during the process. At this scale, thermal problem is generally reduced to a simple conduction problem where the laser input is represented by an equivalent moving heat source [5,6]. As the energy input is approximated, the predicted mechanical behaviour is sometimes far from reality.

Consequently, in order to make the bridge between these two scales, a new mesoscopic approach is proposed, based on the pioneering works of Dal et al. (2016) [7] and Chen et al. (2017) [8]. This intermediate methodology intends to bridge the gap between the fine thermo-hydrodynamic models and the purely thermal macroscopic models. The present proof of concept is performed in a static laser configuration, using the commercial software COMSOL Multiphysics®. The powder bed is represented by a homogeneous absorbing medium with both homogenized thermal and fluid properties. A bulk heat source is considered when the laser heats the powder bed whereas a surface heat flux is imposed on the surface of the liquid pool. Apparent viscosity and surface tension are attributed to the equivalent medium so that modelling powder densification (due to powder coalescence), melting and spheroidization of the melt pool is made possible by solving compressible Navier-Stokes equations. In addition, thermocapillary effects as well as vaporisation-induced recoil pressure are implemented and experimentally validated, so that realistic thermo-hydrodynamic phenomena are successfully taken into account. This makes the present approach a promising alternative to current multi-physical models, which will be easily transposed into a 3D geometry, in single and multiple LBM tracks configurations.

2 PHYSICAL MODEL

2.1 Principles of the mesoscopic approach

The method treats the powder bed, which is a granular medium, as a homogenized continuous material with a given initial porosity and homogenized thermal and fluid properties (Figure 1a). When the equivalent medium is heated, powder irreversible transformation is handled with a densification function ϕ (Figure 1b), which gives the fraction of powder phase as a function of temperature. The medium properties ψ are then expressed as a function of ϕ, to ensure transition from powder to condensed phase properties:

$$\psi = \phi\psi_{powder} + (1 - \phi)\psi_{condensed} \quad (1)$$

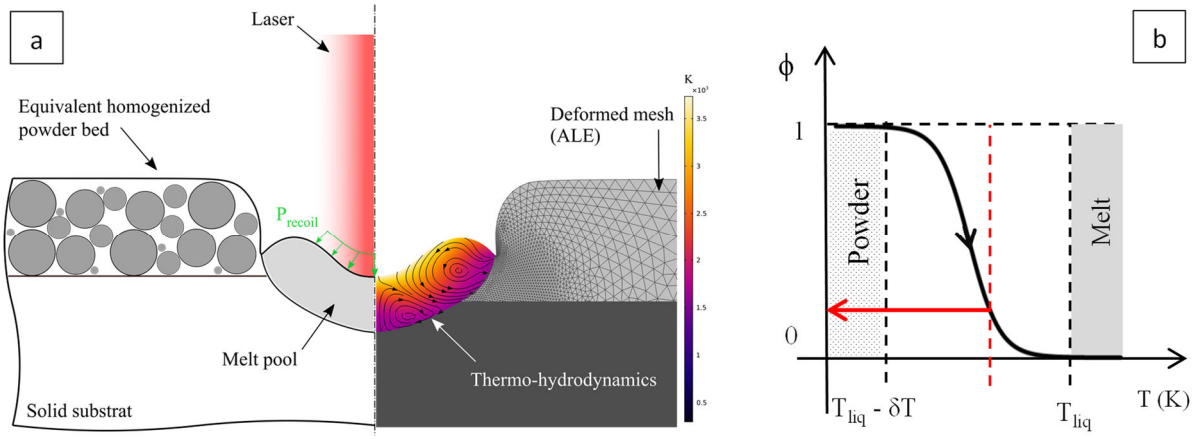

Figure 1: (a) Schematic of the new mesoscopic approach in static laser configuration. (b) Fraction of powder versus temperature. Material transformation is made irreversible, using a hysteresis function (red arrow).

2.2 Governing equations

- *Thermal problem*

Thermal field is computed by solving the energy conservation law in transient condition:

$$\rho c_p^{eq} \frac{\partial T}{\partial t} + \rho c_p (\vec{u} \cdot \vec{\nabla} T) = \vec{\nabla} \cdot (k \vec{\nabla} T) + \phi Q \tag{2}$$

where c_p, ρ, and k are respectively the specific heat, the density and the conductivity of the different phases and Q is the laser heat source. Latent heat of melting L_m is introduced thanks to an equivalent specific heat [9]:

$$c_p^{eq} = c_p + \frac{L_m}{\sqrt{\pi \Delta T^2}} exp\left[-\frac{(T - T_m)^2}{\Delta T^2}\right] \tag{3}$$

where $T_m = 0.5(T_{liq}+T_{sol})$ is the "melting" temperature and $2\Delta T = (T_{liq}-T_{sol})$ is the melting/solidification interval. Regarding the laser source, two cases should be considered, whether the equivalent medium is in powder form or in condensed state. Nevertheless, in both cases, a Gaussian heat flux is imposed on the domain upper boundary [EC] (Figure 2):

$$I_{laser} = A cos(\theta) \frac{P}{\pi R_0^2} exp\left(-\frac{2r^2}{R_0^2}\right) g(t) \tag{4}$$

where A is the material absorptivity, θ is the laser incident angle relative to the material/vapour interface; P and R_0 are the laser power and radius respectively. In addition, $g(t) = 1 – exp(-t/\tau)$ is the temporal profile of the laser pulse, with a characteristic rise time $\tau = 150$ µs.

In the first case, when the irradiated material is in powder state, Gusarov et al. (2009) [10] demonstrated that the powder bed could be approximated to a homogeneous absorbing-scattering medium. Actually, when the laser beam interacts with loose powder, the incident beam penetrates in the bulk medium as it is reflected several times by the powder grains. More recently, Dayal et al. (2017) [11] confirmed this behaviour by means of ray-tracing simulations. Consequently, laser input should be modelled as a bulk heat source, which penetrates in the

powder layer depth. Gusarov et al. proposed an analytical law, which expresses Q as a function of the powder average diameter, the bed porosity and the bed depth. Here, the authors used instead the Beer-Lambert law, which is easier to implement in a finite element code and which gives similar results:

$$Q = \frac{\partial I}{\partial z} = \alpha I \tag{5}$$

where α is the extinction coefficient and I is the heat flux which decays exponentially with the bed depth. Notice that in equation (2), the laser bulk heat source term Q is weighted by the function ϕ, to unsure it only applies in the powder.

In the second case, when the powder is melted, the bulk heat source is not applied anymore ($\phi = 0$) and the laser input reduces to a heat flux on boundary [EC] (Figure 2):

$$k\vec{\nabla}T \cdot (-\vec{n}) = (1 - \phi)I_{laser} - \varphi_{losses} \tag{6}$$

where φ_{losses} contains the heat lost by vaporization, radiation and convection.

Here, the authors should make a remark regarding the chosen heat source model. In practice, it is observed that the laser beam interacts mostly with the melt pool during the process in the steady state regime [12]. The powder bed melts almost instantaneously (≈ 10 µs) at the very first interaction with the laser beam and then the surrounding powder is melted by contact with the melt pool. So one could argue that, as the melting time is negligible compared to the dwell time (≈ 100 µs), it is not necessary to include the first heating stage with the bulk heat source – especially in a moving laser source configuration. This objection would be physically founded. However numerically speaking, our equivalent powder medium has a relatively small thermal diffusivity. Hence, imposing a high heat flux prior to densification would require smaller elements and time steps (and thus longer computational times) to avoid numerical thermal undershoot. Therefore, this approach is also a convenient way to ensure numerical stability.

In addition, heat lost by vaporization equals to the product of the latent heat of vaporisation L_V and the evaporation mass flux. The latter is commonly expressed thanks to the Hertz-Langmuir equation [13]:

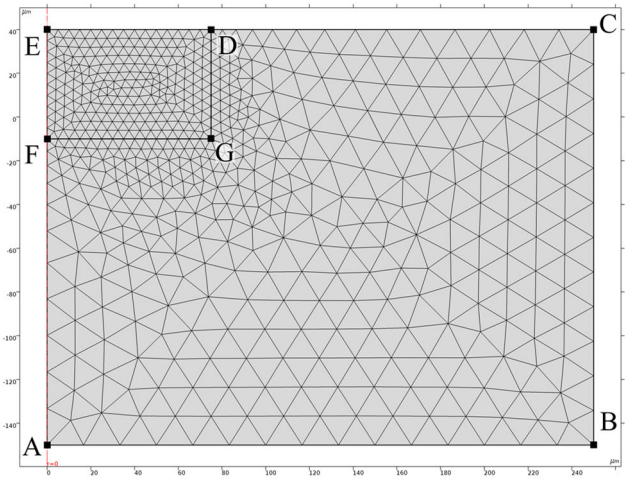

Figure 2: Initial geometry and mesh. Notice that here the mesh has voluntary been coarsen to lighten the figure. Mesh is refined down to 1µm in the subdomain [DEFG].

$$\dot{m} = (1 - \beta_R)\sqrt{\frac{M}{2\pi RT}}P_{sat}(T) \tag{7}$$

where β_R is the retro-diffusion coefficient (i.e. the fraction of vaporized particles which re-condensates when they interact with the surrounding particles), M is the molar mass of the vaporised species and P_{sat} is the saturated vapour pressure. P_{sat} is calculated thanks to the Clausius-Clapeyron law:

$$P_{sat}(T) = P_{atm}exp\left[\frac{ML_v}{RT_V}\left(1 - \frac{T_V}{T}\right)\right] \tag{8}$$

where P_{atm} is the atmospheric pressure and T_V is the boiling point at atmospheric pressure.

In previous works [14,15], we have explained that equation (7) could not be consistently used as it is, because the Hertz-Langmuir law is valid only in vacuum or at temperature much greater than the boiling point, when vaporization is strong enough to expel the surrounding ambient gas. In these cases, β_R tends toward 0.18 [16,17]. Pang et al. (2015) [18] and later Girardot et al. (2017) [19] generalized equation (7) to account for the ambient pressure effects in the whole temperature range. The authors actually followed their recommendations. For conciseness purpose, we will not provide more details here, please report to the cited papers.

Finally, the external boundaries [AB] and [BC] are sufficiently far from the heat source to be set as adiabatic.

- *Fluid flow problem*

At the laser intensities involved in LBM ($I \gtrsim 1$ MW/cm²), similar to laser welding, Semak and Matsunawa (1997) [20] clearly demonstrated that such a process is thermally limited (at steady state) by melt pool convection driven by vaporization-induced recoil pressure. Thanks to their so-called "piston" model, they have estimated that at this intensity order of magnitude, 70% to 90% of the laser energy is exchanged by convection [20]. It is thus of a major importance to compute fluid flow with maximum fidelity.

Fluid flow problem is thus established by solving mass and momentum conservation laws in compressible form to allow powder densification:

$$\frac{\partial \rho}{\partial t} + \vec{\nabla} \cdot (\rho \vec{u}) = 0 \tag{9}$$

$$\rho \frac{\partial \vec{u}}{\partial t} + \rho(\vec{u} \cdot \vec{\nabla})\vec{u} = \vec{\nabla} \cdot \left\{-pI + \mu\left[\vec{\nabla}\vec{u} + (\vec{\nabla}\vec{u})^T\right] - \frac{2}{3}(\vec{\nabla} \cdot \vec{u})I\right\} + K\vec{u} + \rho\vec{g} \tag{10}$$

where μ is the dynamic viscosity and K is a Darcy penalization term, which allows computing the solid/liquid transition in the substrate [21]:

$$K = C_1 \frac{(1 - f_{liq})^2}{f_{liq}^3 + C_2} \tag{11}$$

where f_{liq} is the liquid fraction, C_1 and C_2 are numerical constants tailored to penalize velocity in the solid. In the powder bed, the powder/liquid transition is handled with the ϕ-dependant dynamic viscosity [8].

The melt pool hydrodynamics is driven by different forces applied to the liquid/vapour interface, namely the recoil pressure, surface tension and thermocapillary shear stress:

$$\left(-pI + \mu\left[\vec{\nabla}\vec{u} + \left(\vec{\nabla}\vec{u}\right)^T\right] - \frac{2}{3}\left(\vec{\nabla}\cdot\vec{u}\right)I\right)\cdot\vec{n} = -P_{recoil}\cdot\vec{n} + \sigma\kappa\vec{n} + \frac{\partial\sigma}{\partial T}\vec{\nabla}_S T \quad (12)$$

where the recoil pressure is commonly expressed by [13]:

$$P_{recoil}(T) = \frac{1}{2}(1+\beta_R)P_{sat}(T) \quad (13)$$

As for the vaporization mass flux, we use Pang's recommendations to account for the ambient pressure effects on the recoil pressure [18].

Finally, no slip boundary condition is applied on boundaries [AB] and [BC].

- *Arbitrary Lagrangian Eulerian Method*

The evolution of the domain free boundary [EC] is tracked using the Arbitrary Lagrangian Eulerian (ALE) method, pre-implemented in COMSOL Multiphysics®. With this method, the interface vertices follow the fluid movement through equation (14):

$$V_I = \vec{u}_L\cdot\vec{n} \quad (14)$$

where V_I is the interface velocity and $\vec{u}_L\cdot\vec{n}$ is the fluid velocity projected to the normal of the interface. Interface displacement is then propagated throughout the domain, following the so-called Yeoh smoothing method, which looks at minimising mesh deformation energy [22].

3 MATERIALS PROPERTIES

In the present paper, we present two cases of static laser-matter interaction, with and without powder bed. Except for the thermal conductivity, the initial powder bed properties are calculated as the weighted average of the powder grain properties (Inconel 625®) and the interstitial gas properties (argon):

$$\psi_{powder} = \varepsilon\psi_{argon} + (1-\varepsilon)\psi_{IN625} \quad (16)$$

where ε is the powder bed porosity. Thermal conductivity is estimated as one hundredth of the conductivity of the powder grains [23,24]. All the thermophysical properties used during the simulation are summarized in Table 1 and Table 2.

Table 1: Properties of the powder bed.

Properties (unit)		Value
A	Absorptivity powder/liquid	0.6/0.3
ep	Thickness (µm)	40
k	Thermal conductivity ($Wm^{-1}K^{-1}$)	0.27
α	Extinction coefficient (m^{-1})	1/ep
δT	Densification interval (K)	300
ε	Porosity	0.5
µ	Dynamic viscosity (Pa.s)	15
σ	Surface tension ($N.m^{-1}$)	0.01

Table 2: Thermophysical properties and parameters used in the simulation [25,26].

Properties (unit)		IN625	Argon
c_p	Specific heat ($J.kg^{-1}.K^{-1}$)	680	520
k	Thermal conductivity ($W.m^{-1}.K^{-1}$)	26.9	1.7E-2
L_m	Latent heat of melting ($kJ.kg^{-1}$)	270	
L_V	Latent heat of vaporization ($kJ.kg^{-1}$)	6294	
M	Molar mass ($g.mol^{-1}$)	59.47	
T_{sol}	Solidus temperature (K)	1533	
T_{liq}	Solidus temperature (K)	1609	
T_V	Boiling temperature (K)	3190	
$\gamma = \partial\sigma/\partial T$	Thermocapillary coefficient ($mN.m^{-1}.K^{-1}$)	0.11	
μ	Dynamic viscosity (Pa.s)	2E-3	
ρ	Density ($kg.m^{-3}$)	7886	1.6
σ	Surface tension ($N.m^{-1}$)	1.842	

4 APPLICATION CASES

Prior to modelling the case of powder bed fusion, we should check if our physical model is able to describe correctly the melt pool thermo-hydrodynamics, independently to the powder bed aspect. A preliminary study is thus the case of laser spot welding (i.e. static shooting on plates).

The computational domain with the mesh is shown in Figure 2. To optimize mesh deformation via the ALE method, we have defined a single computational domain where the transition from the substrate to the powder bed is smoothly set, thanks to a Heaviside function. With a two-domain strategy (Figure 3a), the deformed mesh volume would be restrained to the powder layer. With the single-domain strategy (Figure 3b), mesh deforms across the materials domains and elements distortion is propagated throughout the whole volume.

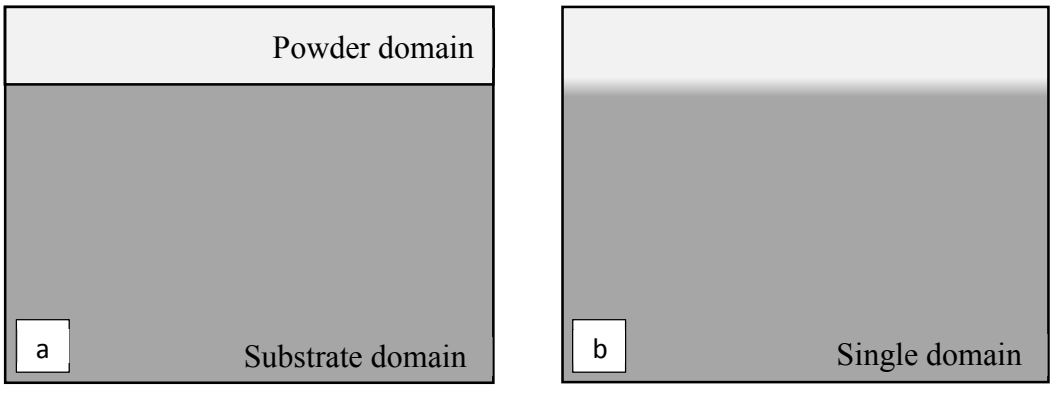

Figure 3: Configuration of the computational domain. (a) Each material (powder/substrate) has its own geometrical domain. (b) There is only one geometrical domain with a smooth transition between the powder layer and the substrate.

Mesh is locally refined, down to 1 µm, around the laser-material interaction zone, where a fine discretization is needed to compute thermal gradient and fluid flow accurately, and where most mesh distortion is expected. With such a mesh, approximately 100,000 degrees of freedom have to be solved. The time step is fixed to 10^{-6} s, using a Backward Euler temporal scheme (BDF, order 1). The problem is solved using the direct PARDISO solver.

Finally, computation took about 3h to simulate 0.1 ms of laser shot with powder, using 8 cores of a Dell® workstation (CPU: Intel® Xeon® @3.2 GHz, RAM: 128 Go).

5 RESULTS

5.1 Case without powder

Below are presented the results of a series of laser spot welding simulations and experiments. We compare on Figure 4a, the macrograph of a fused zone obtained with a 3 ms-long static shot performed on an Inconel 625® plate with a Yb-YAG laser. The focal spot is set to 205 µm and the incident power is 700 W. The shape of the melt pool predicted by finite element method agrees well with the final shape of the fused zone. The temperature of the melt pool free surface, on a width equivalent to the laser spot diameter, is around 3500 K, which is superior to the boiling point at atmospheric pressure (T_V = 3190 K). Consequently, the pressure difference between the centre ($\approx P_{atm} + P_{recoil}$) and the sides ($P_{atm}$) of the melt pool, induces a depression zone (keyhole) which controls the depth of the fused zone. As highlighted by the white streamlines, the melt pool is fed by the solid from the bottom and liquid metal is driven by the recoil pressure, from the centre of the interaction zone to the rim of the melt pool. A small melt volume in the bottom centre of the interaction zone is thus sheared by this ejected melt, generating a small recirculation zone. A second recirculation zone is created at the vicinity of the liquid/solid transition, due to thermocapillary shear stress. This local vortex increases the melt penetration in the solid, hence increasing the local melt pool width.

In addition Figure 4b compares, for different laser incident intensities, the fused zone width and depth predicted by our model and obtained experimentally. Within this intensity range, our model predicts the dimensions of the fused zone with an average error inferior than 10% (5 % for the width and 7% for the depth), which is very satisfying.

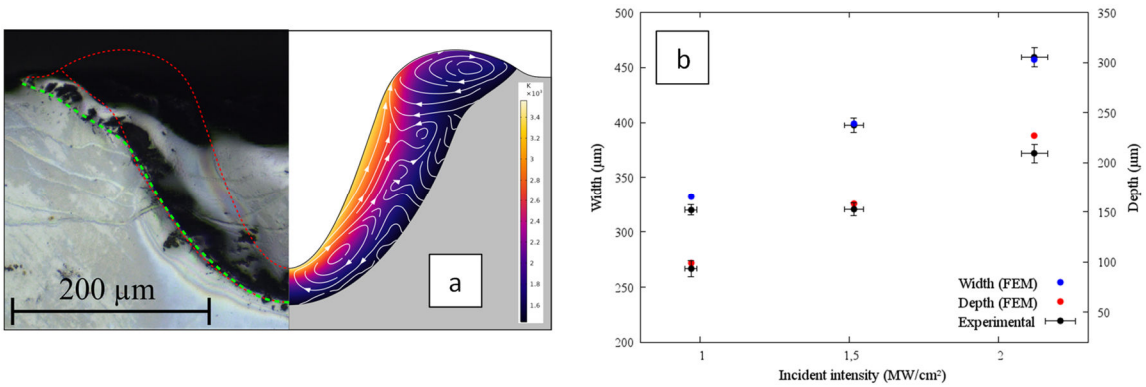

Figure 4: (a) Numerical melt pool compared to the macrograph of the fused zone obtained in the same conditions (P = 700 W, R_0 = 102.5 µm, t = 3 ms). (b) Comparison of the dimensions of the experimental fused zones and the numerical melt pool for different incident intensities.

5.2 Case with powder

Our model presents a good ability to take into account the role of recoil pressure on melt pool hydrodynamics and to predict the shape and the dimensions of the fused zone. Now the study should be focused on the equivalent powder bed.

Figure 5 gives the dynamics of powder bed melting, obtained with a 0.1 ms-long static laser shot, with a focal spot set to 50 µm (typical to LBM) and an incident powder of 250 W. The melting sequence can be decomposed in three steps.

Firstly, during the first tens of microseconds, the equivalent powder bed densifies and melts. The powder volume under the laser spot hence collapses (Figure 5a). Physically speaking, powder densification is due to the melting of individual powder grains which coalesce. A good illustration is given by Körner's simulations [27]. Here, this mechanism is handled with a variation of the equivalent powder bed density with temperature, via the function ϕ. Note that for numerical stability reasons, we have used an artificial densification interval $\delta T = 300$ K, which is larger than the melting interval $2\Delta T = 76$ K. Hence, in our model, densification starts before melting, which is not physical – here, regarding the melting time scale, we do not expect for solid sintering to occur. Nevertheless, this numerical artifice should not have a significant impact at the scale of the LBM bead as it is restrained to short time and length scales.

Secondly, the melt pool created gets it spherical shape due to surface tension (Figure 5b). With our equivalent approach, this is possible because we attribute to the powder, a sufficiently low surface tension (one hundredth of the liquid surface tension), so that powder has no mechanical effect on the melt pool. The melt pool is free to spheroidize. Physically speaking, shaping of the fusion zone is governed by the balance between the melted grain inertia and surface tension. The time scale for the melt pool shaping is given by the Rayleigh time $t_{ray} = (\rho D^3/\sigma)^{1/2}$, which is of the order of 10^{-5}-10^{-4} s for metals [27].

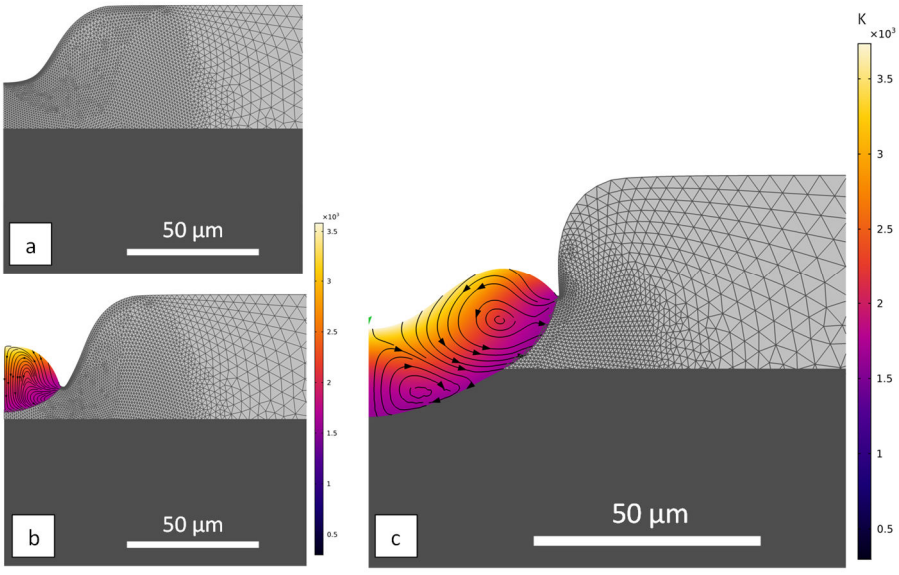

Figure 5: (a) Densification of the powder bed (t ≈ 50 µs). (b) Spheroidization of the melt pool, prior to vaporisation (t ≈ 65 µs). (c) Vaporisation: the melt pool is deflected by the recoil pressure (t ≈ 80 µs).

Finally, the melt surface temperature rapidly reaches the boiling point, after about 65 µs. The spherical melt pool is deformed by the recoil pressure, which favours its penetration in the substrate underneath (Figure 5c).

6 CONCLUSION AND PERSPECTIVES

An original mesoscopic method has been proposed to simulate laser-material interaction during LBM. This new methodology, which treats the powder bed as an equivalent homogeneous medium, has proven to be efficient in modelling hydrodynamics phenomena associated to powder bed fusion – densification, melting and vaporisation – without resorting to the granular description. It is believed that this method is a good alternative to current state-of-the-art multi-physical models as it reduces computational effort associated to meshing granular media. Without powder, the model reduces to the case of laser spot welding, which was successfully validated with experiments.

The next step will be to transpose the current model into a 3D geometry, to simulate a single LBM pass. The shape and dimensions of the obtained bead will be confronted to experiments and to numerical results provided by an alternative level-set approach developed at Mines ParisTech [28], in a context of a collaborative study.

REFERENCES

[1] Dal M and Fabbro R 2016 [INVITED] An overview of the state of art in laser welding simulation *Opt. Laser Technol.* **78** 2–14

[2] Francois M M, Sun A, King W E, Henson N J, Tourret D, Bronkhorst C A, Carlson N N, Newman C K, Haut T, Bakosi J, Gibbs J W, Livescu V, Vander Wiel S A, Clarke A J, Schraad M W, Blacker T, Lim H, Rodgers T, Owen S, Abdeljawad F, Madison J, Anderson A T, Fattebert J L, Ferencz R M, Hodge N E, Khairallah S A and Walton O 2017 Modeling of additive manufacturing processes for metals: Challenges and opportunities *Curr. Opin. Solid State Mater. Sci.* **21** 198–206

[3] Khairallah S A, Anderson A T, Rubenchik A and King W E 2016 Laser powder-bed fusion additive manufacturing: Physics of complex melt flow and formation mechanisms of pores, spatter, and denudation zones *Acta Mater.* **108** 36–45

[4] Tang M, Pistorius P C and Beuth J L 2017 Prediction of lack-of-fusion porosity for powder bed fusion *Addit. Manuf.* **14** 39–48

[5] Papadakis L, Loizou A, Risse J and Schrage J 2014 Numerical computation of component shape distortion manufactured by Selective Laser Melting *Procedia CIRP* **18** 90–5

[6] B Y Z and Guillemot G 2017 Macroscopic Finite Element Thermal Modelling of Selective Laser Melting for IN718 Real Part Geometries Yancheng *Ind. Addit. Manuf. - Proc. Addit. Manuf. Prod. Appl. - AMPA2017*

[7] Dal M, Peyre P, Gunenthiram V and Schneider M 2016 A New Equivalent Approach For Additive Layer Manufactring (ALM) Numerical Modelling *ICALEO Proceedings*

[8] Chen Q, Guillemot G, Gandin C-A and Bellet M 2017 Three-dimensional finite element thermomechanical modeling of additive manufacturing by selective laser melting for ceramic materials *Addit. Manuf.* **16** 124–37

[9] Bonacina C, Comini G, Fasano A and Primicerio M 1973 Numerical solution of

phase-change problems *Int. J. Heat Mass Transf.* **16** 1825–32
[10] Gusarov A V., Yadroitsev I, Bertrand P and Smurov I 2009 Model of Radiation and Heat Transfer in Laser-Powder Interaction Zone at Selective Laser Melting *J. Heat Transfer* **131** 072101
[11] Dayal R and Gambaryan-Roisman T 2017 Heat transfer in granular medium for application to selective laser melting: A numerical study *Int. J. Therm. Sci.* **113** 38–50
[12] Scipioni Bertoli U, Wolfer A J, Matthews M J, Delplanque J P R and Schoenung J M 2017 On the limitations of Volumetric Energy Density as a design parameter for Selective Laser Melting *Mater. Des.* **113** 331–40
[13] Samokhin A A 1990 *Effect of Laser Radiation on Absorbing Condensed Matter* ed V B Fedorov (Nova Science Publishers)
[14] Mayi Y A, Dal M, Peyre P, Bellet M, Metton C, Moriconi C and Fabbro R 2018 Two-Phase Flow Modelling of Metal Vaporisation under Static Laser Shot using a Double Domain ALE Method – A Feasibility Study *Proceedings of the 2018 COMSOL Conference* (Lausanne)
[15] Mayi Y A, Dal M, Peyre P, Bellet M, Metton C, Moriconi C and Fabbro R 2019 Effets de la Nature du Gaz Ambiant sur les Ecoulements Induits lors de la Vaporisation d'un Alliage Métallique sous Faisceau Laser
[16] Anisimov S I 1968 Vaporization of metal absorbing laser radiation *Sov. Phys. JETP* **27** 182–3
[17] Knight C J 1979 Theoretical Modeling of Rapid Surface Vaporization with Back Pressure *AIAA J.* **17** 519–23
[18] Pang S, Hirano K, Fabbro R and Jiang T 2015 Explanation of penetration depth variation during laser welding under variable ambient pressure *J. Laser Appl.* **27** 022007
[19] Girardot J, Lorong P, Illoul L, Ranc N, Schneider M and Favier V 2017 Modeling laser drilling in percussion regime using constraint natural element method *Int. J. Mater. Form.* **10** 205–19
[20] Semak V and Matsunawa A 1997 The role of recoil pressure in energy balance during laser materials processing *J. Phys. D. Appl. Phys.* **30** 2541–52
[21] Voller V R and Prakash C 1987 A fixed grid numerical modelling methodology for convection-diffusion mushy region phase-change problems *Int. J. Heat Mass Transf.* **30** 1709–19
[22] Comsol Mutliphysics User's Guide 2018 Comsol Multiphysics User's Guide
[23] Zehner P and U Schlünder E 1970 Thermal conductivity of granular materials at moderate temperatures *Chem Ing-Tech* **42** 933–41
[24] Rombouts M, Froyen L, Gusarov A V., Bentefour E H and Glorieux C 2005 Photopyroelectric measurement of thermal conductivity of metallic powders *J. Appl. Phys.* **97**
[25] Mills K C 2002 *Recommended values of thermophysical properties for selected commercial alloys* (Cambridge: Woodhead Publishing Limited)
[26] Anon Gas Encyclopedia Air Liquide | Air Liquide
[27] Körner C, Bauereiß A and Attar E 2013 Fundamental consolidation mechanisms during selective beam melting of powders *Model. Simul. Mater. Sci. Eng.* **21**
[28] Queva A, Mayi Y, Bellet M, Guillemot G, Peyre P, Dal M, Moriconi C and Metton C

2019 Thermo-mechanical simulation of track development in the Laser Beam Melting process - Effect of laser-metal interaction *IOP Conf. Ser. Mater. Sci. Eng.* **529** 012005